Second order scheme for open channel flow

Roshan Sharma
Telemark University College

June 23, 2015

Contents

Preface

In the search for a numerical scheme which: (i) is semi-descrete in nature (only space discritization) so that built-in ODE solvers in MATLAB or Modelica can be used, (ii) can handle dry bed conditions (island or dry shoals), (iii) is Reimenn-solver free so that it can be used as a black box solver, (iv) is higher order yet Total Variation Diminishing (TVD), (v) can handle bed discontinuities (discontinuity in bottom topography), (vi) can handle width discontinuities, (vii) is well-balanced and preserves the static equilibria (lake-at-rest), and (viii) can be modified to support higher order polynomial reconstruction, a second order accurate scheme known as Kurganov-Petrova central upwind scheme is presented. The scheme is implemented in MATLAB and a case study of a run-of-river power plant is described.

Chapter 1

Introduction

Shallow water equations also known as Saint Venant equations (for one dimensional case) are hyperbolic partial differential equations. A common way of expressing the Saint Venant equation with the source term is

$$\frac{\partial U(x,t)}{\partial t} + \frac{\partial F(x,t,U)}{\partial x} = S(x,t,U) \tag{1.1}$$

where U is the vector of conserved variables, F is the vector of fluxes and S is the source terms which are expressed as

$$U = (A,Q)^T \tag{1.2}$$

$$F = \left(Q, \frac{Q^2}{A} + gI_1\right)^T \tag{1.3}$$

$$S = \left(0, gI_2 + gA\left(S_0 - S_f\right)\right)^T. \tag{1.4}$$

Here, A is the wetted cross sectional area, Q is the discharge, g is the acceleration due to gravity, S_0 is the bed slope or bathymetry and S_f is the friction term. The bathymetry shows the variation of the bed along the length of the open channel (see Figure 1.1). It is expressed as the spatial partial derivative of the bottom elevation B as

$$S_0 = -\frac{\partial B}{\partial x}. \tag{1.5}$$

I_1 represents the hydrostatic pressure force term and is expressed as

$$I_1(x,A) = \int_0^{h(x,A)} \left(h(x,A) - \widetilde{z}\right) w(x,\widetilde{z}) d\widetilde{z}. \tag{1.6}$$

Here, $h(x,A)$ is the water depth and $w(x,\widetilde{z})$ is the width of the channel at an arbitrary position $\widetilde{z}$ from the datum. The width of the channel is written as

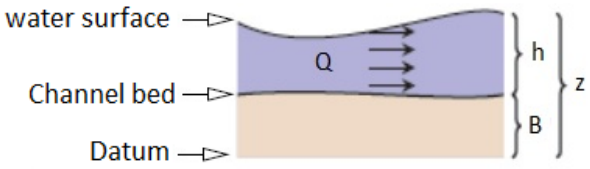

Figure 1.1: Schematic of an open channel flow

$$w(x,\widetilde{z}) = \frac{\partial A(x,t)}{\partial \widetilde{z}}. \tag{1.7}$$

I_2 represents the pressure forces in a volume of constant depth h due to longitudinal width variations.

$$I_2(x,A) = \int_0^{h(x,A)} (h(x,A) - \widetilde{z}) \frac{\partial w(x,\widetilde{z})}{\partial x} d\widetilde{z}. \tag{1.8}$$

For rectangular channel, the side slope $S_L = 0$. Then,

$$I_1 = \frac{h^2 w}{2} = \frac{A^2}{2w} \tag{1.9}$$

$$I_2 = \frac{A^2}{2w^2}\frac{dw}{dx}. \tag{1.10}$$

For a rectangular channel with constant width, $I_2 = 0$. For a trapezoidal channel with side slope S_L and with base width W,

$$I_1 = h^2\left(\frac{W}{2} + h\frac{S_L}{3}\right) \tag{1.11}$$

$$I_2 = h^2\left(\frac{1}{2}\frac{dW}{dx} + \frac{h}{3}\frac{dS_L}{dx}\right). \tag{1.12}$$

For a trapezoidal channel with constant side slope and constant base width, $I_2 = 0$. For a Newtonian fluid[1], the friction term S_f can be represented[2] by using Manning's roughness coefficient n as

$$S_f = \frac{Q\,|Q|\,n^2 P^{\frac{4}{3}}}{A^{\frac{10}{3}}} \tag{1.13}$$

with P being the wetted perimeter. For a rectangular channel $P = w + 2h$.For a rectangular channel with a constant width w, a very common expression of the system is

[1] For a non-Newtonian fluid, the friction slope can be calculated using $Herschel - Bulkley$ model.
[2] Other representations or forms of the friction slope S_f can also be used.

$$\frac{\partial A}{\partial t} + \frac{\partial Q}{\partial x} = 0 \tag{1.14}$$

$$\frac{\partial Q}{\partial t} + \frac{\partial}{\partial x}\left(\frac{Q^2}{A} + \frac{gA^2}{2w}\right) = gA(S_0 - S_f). \tag{1.15}$$

If $F = F(U, x, t)$,equation 1.1 can be written in the form

$$\frac{\partial U}{\partial t} + J\frac{\partial U}{\partial x} = S \tag{1.16}$$

where J is the Jacobian matrix of the system and is given by

$$J = \begin{bmatrix} 0 & 1 \\ c^2 - u^2 & 2u \end{bmatrix}. \tag{1.17}$$

The cross section averaged water velocity $u = \frac{Q}{A} = \frac{hu}{h}$. The celerity[3] of the small amplitude surface wave $c = \sqrt{gh}$. The eigen values of the Jacobian matrix is

$$\lambda_{1,2} = u \mp \sqrt{gh}. \tag{1.18}$$

The eigen values represent the speed of propagation of the perturbations and hence are the convective wave velocities. A difficulty may occur when dry ($h = 0$) or near dry ($h \sim 0$) bed conditions are to be captured or studied. In such cases, due to numerical oscillations, h may become negative and the numerical computation scheme which uses the eigen values will break down. Thus a good numerical scheme should be able to preserve the positivity property i.e. the computed values of the fluid depth should be nonnegative.

Using $Q = huw = qw$, for a rectangular channel with constant width w, $A = wh$ and $q = hu$, equations 1.14 and 1.15 can be written as

$$\frac{\partial h}{\partial t} + \frac{\partial q}{\partial x} = 0 \tag{1.19}$$

$$\frac{\partial q}{\partial t} + \frac{\partial}{\partial x}\left(hu^2 + \frac{g}{2}h^2\right) = -gh\frac{\partial B}{\partial x} - \frac{gn^2 q\,|q|\,(w+2h)^{\frac{4}{3}}}{w^{\frac{4}{3}}}\frac{1}{h^{\frac{7}{3}}}. \tag{1.20}$$

When $Q = 0$ or $q = 0$, the system should exhibit stationary steady state solution (lake at rest condition) i.e. it should be well-balanced. When the system is in the stationary steady state, it is very important to understand that the water surface $h + B = z$ is constant, not the water depth h. Thus, to preserve the well-balanced and positivity conditions, change of variables from (h, hu) to $(z = h + B, hu)$ is performed. An equivalent representation of the system in terms of the water surface $z = h + B$ and the discharge $q = hu$ is

[3] Celerity is analogous to the speed of sound in gases and contains the essence of the compressibility associated to the deformability of the free surface.

$$\frac{\partial z}{\partial t} + \frac{\partial q}{\partial t} = 0 \tag{1.21}$$

$$\begin{aligned} \frac{\partial q}{\partial t} + \frac{\partial}{\partial x}\left(\frac{q^2}{z-B} + \frac{g}{2}(z-B)^2\right) &= -g(z-B)\frac{\partial B}{\partial x} \\ &\quad - \frac{gn^2 q\,|q|\,(w+2(z-B))^{\frac{4}{3}}}{w^{\frac{4}{3}}}\frac{1}{(z-B)^{\frac{7}{3}}}. \end{aligned} \tag{1.22}$$

In the compact form, equations 1.21 and 1.22 can be written as

$$\frac{\partial U}{\partial t} + \frac{\partial F}{\partial x} = S \tag{1.23}$$

with

$$U := (z, q)^T \tag{1.24}$$

$$F := \left(q, \frac{q^2}{z-B} + \frac{g}{2}(z-B)^2\right)^T \tag{1.25}$$

$$S := \left(0, -g(z-B)\frac{\partial B}{\partial x} - \frac{gn^2 q\,|q|\,(w+2(z-B))^{\frac{4}{3}}}{w^{\frac{4}{3}}}\frac{1}{(z-B)^{\frac{7}{3}}}\right)^T. \tag{1.26}$$

Chapter 2

Finite Volume Method

Conservation laws are usually solved by finite-volume methods. With the finite volume method, we divide the grid into small control volumes or control cells and then apply the conservation laws of equation 1.23 to each cell. Since equation 1.23 hold for any subset $k \subset \Omega \subset \mathbb{R}^n$,it holds for any cell in some defined grid. For simplicity, we consider one spatial dimension only. However, the concept can be equally extended to higher spatial dimensions.

2.1 Control Cell and notations

Let us consider a single cell of a grid as shown in Figure 2.1.

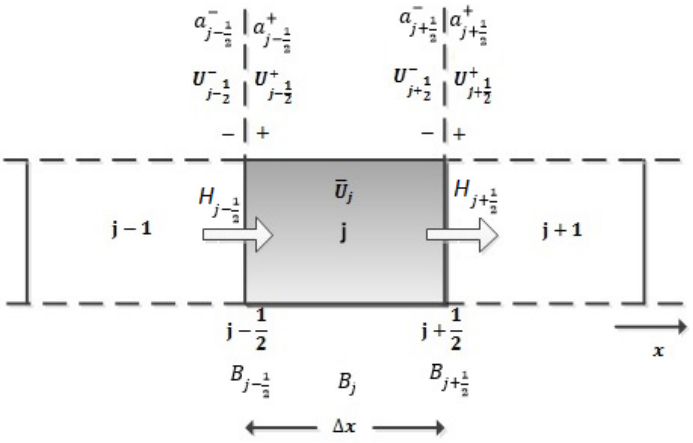

Figure 2.1: Control volume/cell and notations

The given cell is denoted by j i.e. it is the j^{th} cell. Cell average is calculated at the center of the cell and $\overline{U}_j$ denotes the average values of the conserved variables. The left and the right interfaces of the cell are denoted by $j - \frac{1}{2}$ and $j + \frac{1}{2}$ respectively. At each cell interface, the right(+)/left(-) point values are reconstructed. As an example,

$U^-_{j-\frac{1}{2}}$ denotes the value of U slightly left of the left interface, $U^+_{j-\frac{1}{2}}$ denotes the value of U slightly right of the left interface, $U^-_{j+\frac{1}{2}}$ denotes the value of U slightly left of the right interface and $U^+_{j+\frac{1}{2}}$ denotes the value of U slightly right of the right interface. As we will see later, $U^\pm_{j\pm\frac{1}{2}}$ are actually the end point values of a piecewise reconstructed polynomial. Similarly, $B_{j\pm\frac{1}{2}}$ represents the channel bed elevation at the left and the right interfaces of the cell respectively. B_j represents the channel bed elevation at the cell center. $a^\pm_{j-\frac{1}{2}}$ denotes the right and the left sided local speeds of propagation at the left interface of the cell, and $a^\pm_{j+\frac{1}{2}}$ denotes the right and the left sided local speeds of propagation at the right interface of the cell. $a^\pm_{j\pm\frac{1}{2}}$ are obtained from the largest and the smallest eigenvalues of the Jacobian matrix J and are described later in detail.

Let $x_j = j\triangle x$, $j = \cdots, -2, -1, 0, 1, 2, \cdots$ and $t_n = n\triangle t$, $n = 0, 1, 2, \cdots$ be a descritization of the space-time domain (x, t). Let us consider a grid cell in the interval $\left[x_{j-\frac{1}{2}}, x_{j+\frac{1}{2}}\right]$. The cell average at time $t = t_n$ at the grid cell is defined as

$$\overline{U}^n_j = \frac{1}{\triangle x}\int_{x_{j-\frac{1}{2}}}^{x_{j+\frac{1}{2}}} U(x, t_n)dx. \tag{2.1}$$

Let us integrate equation 1.23 on the rectangle $[t_n, t_{n+1}] \times \left[x_{j-\frac{1}{2}}, x_{j+\frac{1}{2}}\right]$ such that

$$\int_{t_n}^{t_{n+1}}\int_{x_{j-\frac{1}{2}}}^{x_{j+\frac{1}{2}}} \frac{\partial U}{\partial t}dxdt + \int_{t_n}^{t_{n+1}}\int_{x_{j-\frac{1}{2}}}^{x_{j+\frac{1}{2}}} \frac{\partial F}{\partial x}dxdt = \int_{t_n}^{t_{n+1}}\int_{x_{j-\frac{1}{2}}}^{x_{j+\frac{1}{2}}} S\ dxdt \tag{2.2}$$

$$\begin{aligned}\int_{t_n}^{t_{n+1}}\int_{x_{j-\frac{1}{2}}}^{x_{j+\frac{1}{2}}} S\ dxdt &= \int_{x_{j-\frac{1}{2}}}^{x_{j+\frac{1}{2}}} U(x, t_{n+1})dx - \int_{x_{j-\frac{1}{2}}}^{x_{j+\frac{1}{2}}} U(x, t_n)dx \\ &\quad + \int_{t_n}^{t_{n+1}} F\left(U(x_{j+\frac{1}{2}}, t)\right)dt - \int_{t_n}^{t_{n+1}} F\left(U(x_{j-\frac{1}{2}}, t)\right)dt.\end{aligned} \tag{2.3}$$

Dividing equation 2.3 by the cell size $\triangle x$ and the time step size $\triangle t$ and using the defination of the cell average from equation 2.1 we get

$$\frac{\overline{U}^{n+1}_j - \overline{U}^n_j}{\triangle t} = -\frac{1}{\triangle t\triangle x}\left[\begin{array}{c}\int_{t_n}^{t_{n+1}} F\left(U(x_{j+\frac{1}{2}}, t)\right)dt - \int_{t_n}^{t_{n+1}} F\left(U(x_{j-\frac{1}{2}}, t)\right)dt \\ + \int_{t_n}^{t_{n+1}}\int_{x_{j-\frac{1}{2}}}^{x_{j+\frac{1}{2}}} S\ dxdt\end{array}\right]. \tag{2.4}$$

By definition,

$$\frac{d}{dt}\overline{U}_j(t) = \lim_{\triangle t\to 0}\frac{\overline{U}^{n+1}_j - \overline{U}^n_j}{\triangle t}. \tag{2.5}$$

Now taking the limit $\triangle t \to 0$ and rearraging, we finally obtain

$$\frac{d}{dt}\overline{U}_j(t) = -\frac{H_{j+\frac{1}{2}}(t) - H_{j-\frac{1}{2}}(t)}{\triangle x} + \overline{S_j}(t) \tag{2.6}$$

where

$$H_{j+\frac{1}{2}}(t) = \lim_{\triangle t \to 0} \frac{1}{\triangle t} \int_{t_n}^{t_{n+1}} F\left(U(x_{j+\frac{1}{2}}, t)\right) dt \tag{2.7}$$

$$H_{j-\frac{1}{2}}(t) = \lim_{\triangle t \to 0} \frac{1}{\triangle t} \int_{t_n}^{t_{n+1}} F\left(U(x_{j-\frac{1}{2}}, t)\right) dt \tag{2.8}$$

$$\overline{S_j}(t) = \lim_{\triangle t \to 0} \frac{1}{\triangle t \triangle x} \int_{t_n}^{t_{n+1}} \int_{x_{j-\frac{1}{2}}}^{x_{j+\frac{1}{2}}} S \; dxdt \approx \frac{1}{\triangle x} \int_{x_{j-\frac{1}{2}}}^{x_{j+\frac{1}{2}}} S(U(x,t), B(x)) \; dx \tag{2.9}$$

Provided that we find an adequate numerical approximation to the time integral, equation 2.6 provides a numerical scheme for the hyperbolic conservation law.

2.2 REA Algorithm

One of the ways of building up a high-resolution numerical method providing high-order accuracy is to apply the REA algoirthm: Reconstruct, Evolve, Average which is a three-steps algorithm to advance the solution of the semi-discrete conservation law of equation 2.6.

1. Reconstruct:

The cell averages $\overline{U}$ are used to obtain the end point values of the conserved variable U. The end point values are the values of U at the left and right interfaces of a given cell i.e. $U^{\pm}_{j\pm\frac{1}{2}}$ are the end point values. For this, we reconstruct a polynomial

$$\widetilde{U}_j(x) = p(x), \qquad x_{j-\frac{1}{2}} \leq x \leq x_{j+\frac{1}{2}} \tag{2.10}$$

for each cell and use it obtain $U^{\pm}_{j\pm\frac{1}{2}}$ which in turn are used to evaluate the flux interface integrals $H_{j\pm\frac{1}{2}}$. The first order reconstructed polynomial for each cell would be to set $\widetilde{U}_j(x) = \overline{U}_j$ i.e. we approximate the conserved variables by a piecewise constant function. The second order reconstructed polynomial would be to approximate the conserved variables by a piecewise linear function at each cell in the grid as shown in Figure 2.2

If s_j represents the slope of the piecewise linear function for the j^{th} cell, it can be expressed as,

$$p_j(x) = \widetilde{U}_j(x) = \overline{U}_j + s_j(x - x_j), \qquad x_{j-\frac{1}{2}} \leq x \leq x_{j+\frac{1}{2}}. \tag{2.11}$$

Infact the order of the proposed scheme depends on the order of the reconstructed polynomial $p_j(x)$. A third order scheme employ a piecewise quadratic approximation

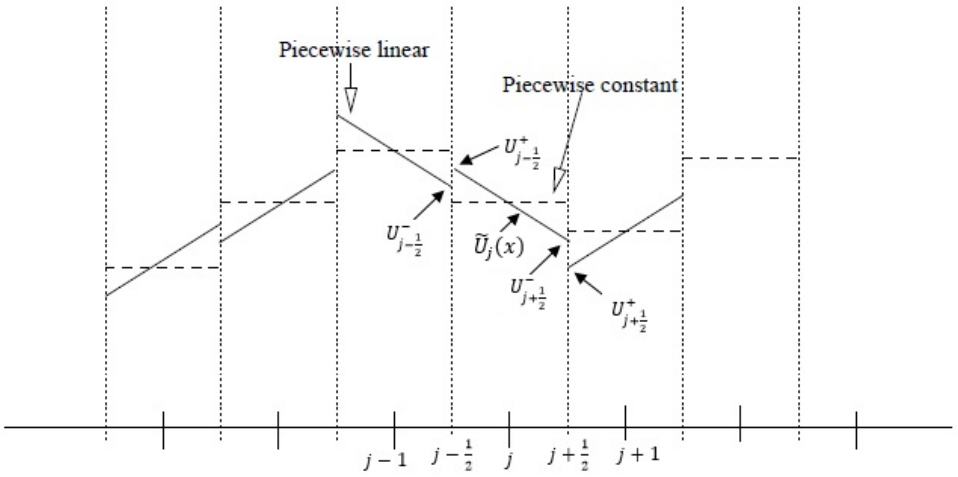

Figure 2.2: Piecewise linear and constant approximation at each cell in a 1D grid

(see [1] and [2] for details) . It is also possible to use the essentially nonoscillatory (ENO) reconstruction (see [3] and [4]) and the W(weighted)ENO reconstruction (see [5], [6], [7] and [8] for more details).

From Godunov's order barrier theorem [9], a scheme which produces nonoscillatory solutions is to the most first order accurate. This means that the second order scheme may produce spurious osciallations near discontinuous points. A good higher order scheme should minimize the spurious oscillations and be total variation diminishing (TVD). Total variation (TV) is given by

$$TV = \int \left| \frac{\partial U}{\partial x} \right| dx = \sum_j |U_{j+1} - U_j| \,. \tag{2.12}$$

A numerical scheme is said to be TVD if

$$TV\left(U(x,\tau)\right) \leq TV\left(U(x,t)\right), \qquad \forall\ t \leq \tau. \tag{2.13}$$

A second order reconstruction should posses these properties and converge with maximal accuracy in smooth areas, but at the same time behave properly around discontinuities. The TVD property is achieved by using a limiting function. For the second order scheme where piecewise linear reconstruction is used, this limiting function is also known as slope limiter. For obtaining the slope s_j of the piecewise linear function $p_j(x)$ of equation 2.11 we have three choices of two point stencils[1] (cells) (from the basic theory of finite difference methods), which are

$$s_j^- = \frac{\overline{U}_j - \overline{U}_{j-1}}{\triangle x_i}, \quad s_j^c = \frac{\overline{U}_{j+1} - \overline{U}_{j-1}}{2\triangle x_i}, \quad s_j^+ = \frac{\overline{U}_{j+1} - \overline{U}_j}{\triangle x_i} \tag{2.14}$$

[1] In plain english, stencil means a thin sheet of card, plastic or metal with a pattern, used to produce the design on the surface below by applying ink or paint through the holes. Here, it means those cells of the grid that are being used to design the slope needed for reconstructing the piecwise linear polynomial.

The choice of S_j is performed in a way that the spurious osciallations are the least. One such limiter function which ensures least oscillations is the minmod limiter (see [10], [11] and [12] for details)

$$s_j = \text{minmod}(s_j^-, s_j^c, s_j^+) = \begin{cases} \min(s_j^-, s_j^c, s_j^+) & if\ s_j^- > 0 \& s_j^c > 0 \& s_j^+ > 0 \\ \max(s_j^-, s_j^c, s_j^+) & if\ s_j^- < 0 \& s_j^c < 0 \& s_j^+ < 0 \\ 0 & otherwise \end{cases} \tag{2.15}$$

There are other types of limiter functions such as *Superbee*, *QUICK*, *Sweby*, *Van Leer*, *Osher* etc. mentioned in literature.

Sumup: The piecewise reconstructed polynomial $\widetilde{U}_j(x)$ (with slope limiter for maintaining the TVD property) is used to obtain the values of $U^{\pm}_{j\pm\frac{1}{2}}$ at the left/right cell interfaces at time $t = t_n$. We then use $U^{\pm}_{j\pm\frac{1}{2}}$ to compute the fluxes $H_{j\pm\frac{1}{2}}(t_n)$ and the source term $\overline{S_j}(t_n)$.

2. Evolve:

From time $t = t_n$, we evolve the reconstructed polynomial $\widetilde{U}_j(x, t_n) = p(x, t_n)$ according to the conservation law of equation 2.6 to obtain $\widetilde{U}_j(x, t_{n+1})$ at time $t = t_{n+1}$.

3. Average:

The average cell value at $t = t_{n+1}$ is then obtained as

$$\overline{U}_j^{n+1} = \frac{1}{\triangle x} \int_{x_{j-\frac{1}{2}}}^{x_{j+\frac{1}{2}}} \widetilde{U}_j(x, t_{n+1}) dx \tag{2.16}$$

The evolving and averaging step can be done by an appropriate TVD preserving Runge-Kutta method. For our implementation, we will use the built-in ODE solvers in MATLAB. Thus the evolving and averaging step is not dicussed in detail here. Detailed information about the TVD preserving RK method are available elsewhere in literature. It is worth mentioning that using a higher order ODE solver (in our case, higher than second order) does not increase the order of the numerical scheme. It is probably better to use an ODE solver having the same order as the order of the numerical scheme.

Chapter 3

Second order Central Upwind scheme

3.1 Introduction

In order to determine the fluxes at the cell interface $H_{j\pm\frac{1}{2}}(t_n)$ and the source term $\overline{S_j}(t_n)$, various schemes are available. We focus on a scheme developed by Alexander Kurganov and Guergana Petrova (here indicated as KP07 scheme). This is a second order scheme which is both well balanced (preserves the stationary steady state by appropriately handling the source term) and also preserves the positivity of the height. It is a Reimann problem[1] solver free scheme (central scheme) while at the same time it takes the advantage of the upwind scheme by utilizing the local, one side speed of propagation (given by the Eigen values of the Jacobian matrix J of equation 1.16) during the calculation of the flux at the cell interfaces.

In this chapter the detailed description of the developement of the scheme and the underlying proofs and theorems are not explained. We simply describe the scheme in a way that is can readily and easily be implemented by the readers (say by using MATLAB/Modelica for their numerical problems). For readers who are interested in the details about the development of the scheme, refer to [13], [14], [15] and [16].

[1] At the cell interfaces, the two one-sided reconstructions of U i.e. $U^+_{j+\frac{1}{2}}$ and $U^-_{j+\frac{1}{2}}$ $\left(or\ U^+_{j-\frac{1}{2}} \text{ and } U^-_{j-\frac{1}{2}}\right)$ are in general not equal, and determining the flux integral is similar to locally solving the Riemann problem. We call a method upwind if it aims to solve the Riemann problem, either exact or by an approximate solver, in order to compute the interface fluxes. In contrast, a central scheme, does not apply any Riemann solvers.

3.2 Numerical scheme

3.2.1 Semi-Descritization

The central-upwind numerical schem is presented for one dimensional case. At first let us re-write the Saint Venant equations that needs to be solved numerically.

$$\frac{\partial U}{\partial t} + \frac{\partial F}{\partial x} = S \tag{3.1}$$

with

$$U : = (z, q)^T \tag{3.2}$$

$$F : = \left(q, \frac{q^2}{z-B} + \frac{g}{2}(z-B)^2\right)^T \tag{3.3}$$

$$S : = \left(0, -g(z-B)\frac{\partial B}{\partial x} - \frac{gn^2 q\,|q|\,(w+2(z-B))^{\frac{4}{3}}}{w^{\frac{4}{3}}}\frac{1}{(z-B)^{\frac{7}{3}}}\right)^T. \tag{3.4}$$

To recall, $z = h + B$ is the water surface elevation with h being the water depth and B being the the channel bed elevation. $q = hu = Q/w$ is the discharge per unit width of the open channel. Let us consider a one dimensional uniform grid with a cell size of $\triangle x$ as shown in Figure 2.1 and a finite volume cell $x_{j-\frac{1}{2}} \leq x_j \leq x_{j+\frac{1}{2}}$. The semi-discrete (time dependent ODEs) central-upwind scheme of equation 3.1 can be written in the following from,

$$\frac{d}{dt}\overline{U}_j(t) = -\frac{H_{j+\frac{1}{2}}(t) - H_{j-\frac{1}{2}}(t)}{\triangle x} + \overline{S_j}(t) \tag{3.5}$$

where the central upwind numerical fluxes $H_{j\pm\frac{1}{2}}(t)$ at the cell interfaces are given by

$$H_{j+\frac{1}{2}}(t) = \frac{a^+_{j+\frac{1}{2}} F\left(U^-_{j+\frac{1}{2}}, B_{j+\frac{1}{2}}\right) - a^-_{j+\frac{1}{2}} F\left(U^+_{j+\frac{1}{2}}, B_{j+\frac{1}{2}}\right)}{a^+_{j+\frac{1}{2}} - a^-_{j+\frac{1}{2}}} + \frac{a^+_{j+\frac{1}{2}} a^-_{j+\frac{1}{2}}}{a^+_{j+\frac{1}{2}} - a^-_{j+\frac{1}{2}}}\left[U^+_{j+\frac{1}{2}} - U^-_{j+\frac{1}{2}}\right] \tag{3.6}$$

$$H_{j-\frac{1}{2}}(t) = \frac{a^+_{j-\frac{1}{2}} F\left(U^-_{j-\frac{1}{2}}, B_{j-\frac{1}{2}}\right) - a^-_{j-\frac{1}{2}} F\left(U^+_{j-\frac{1}{2}}, B_{j-\frac{1}{2}}\right)}{a^+_{j-\frac{1}{2}} - a^-_{j-\frac{1}{2}}} + \frac{a^+_{j-\frac{1}{2}} a^-_{j-\frac{1}{2}}}{a^+_{j-\frac{1}{2}} - a^-_{j-\frac{1}{2}}}\left[U^+_{j-\frac{1}{2}} - U^-_{j-\frac{1}{2}}\right], \tag{3.7}$$

with $a^{\pm}_{j\pm\frac{1}{2}}$ being the one-sided local speeds of propagation.

3.2.2 Piecewise linear reconstruction

Equation 3.5 is initialized with the cell center average values $\overline{U}_j$. However, for calculating the numerical fluxes $H_{j\pm\frac{1}{2}}(t)$ using equations 3.6 and 3.7, the values of $U^{\pm}_{j\pm\frac{1}{2}}$ are needed. These can be calculated as the end points of a piecewise linearly reconstructed function $\widetilde{U}_j(x)$ as

$$\widetilde{U}_j(x) = \overline{U}_j + s_j(x - x_j), \qquad x_{j-\frac{1}{2}} \leq x \leq x_{j+\frac{1}{2}}. \tag{3.8}$$

$U^{\pm}_{j+\frac{1}{2}}$ are the right/left point values at $x = x_{j+\frac{1}{2}}$ i.e.

$$U^{\pm}_{j+\frac{1}{2}} = \widetilde{U}(x_{j+\frac{1}{2}}) = \overline{U}_{j+\frac{1}{2}\pm\frac{1}{2}} \mp \frac{\triangle x}{2} s_{j+\frac{1}{2}\pm\frac{1}{2}}. \tag{3.9}$$

$U^{\pm}_{j-\frac{1}{2}}$ are the right/left point values at $x = x_{j-\frac{1}{2}}$ i.e.

$$U^{\pm}_{j-\frac{1}{2}} = \widetilde{U}(x_{j-\frac{1}{2}}) = \overline{U}_{j-\frac{1}{2}\pm\frac{1}{2}} \mp \frac{\triangle x}{2} s_{j-\frac{1}{2}\pm\frac{1}{2}}. \tag{3.10}$$

Listing them separately we have,

$$U^{-}_{j+\frac{1}{2}} = \overline{U}_j + \frac{\triangle x}{2} s_j \tag{3.11}$$

$$U^{+}_{j+\frac{1}{2}} = \overline{U}_{j+1} - \frac{\triangle x}{2} s_{j+1} \tag{3.12}$$

$$U^{-}_{j-\frac{1}{2}} = \overline{U}_{j-1} + \frac{\triangle x}{2} s_{j-1} \tag{3.13}$$

$$U^{+}_{j-\frac{1}{2}} = \overline{U}_j - \frac{\triangle x}{2} s_j. \tag{3.14}$$

3.2.3 Slope limiter

The slope s_j of the reconstructed function in each cell is computed using a limiter function to obtain a non-oscillatory nature of the reconstruction. The KP07 scheme utilizes the generalized minmod limiter as

$$s^{-}_j = \theta \frac{\overline{U}_j - \overline{U}_{j-1}}{\triangle x_i}, \quad s^{c}_j = \frac{\overline{U}_{j+1} - \overline{U}_{j-1}}{2\triangle x_i}, \quad s^{+}_j = \theta \frac{\overline{U}_{j+1} - \overline{U}_j}{\triangle x_i} \tag{3.15}$$

$$s_j = \text{minmod}(s^{-}_j, s^{c}_j, s^{+}_j) = \begin{cases} \min(s^{-}_j, s^{c}_j, s^{+}_j) & if\ s^{-}_j > 0 \& s^{c}_j > 0 \& s^{+}_j > 0 \\ \max(s^{-}_j, s^{c}_j, s^{+}_j) & if\ s^{-}_j < 0 \& s^{c}_j < 0 \& s^{+}_j < 0 \\ 0 & otherwise \end{cases} \tag{3.16}$$

The parameter $\theta \epsilon [1, 2]$ is used to control or tune the amount of numerical dissipation or numerical viscosity present in the resulting scheme. The larger the value of θ the smaller the numerical dissipation. The value of $\theta = 1.3$ is a good starting point in general.

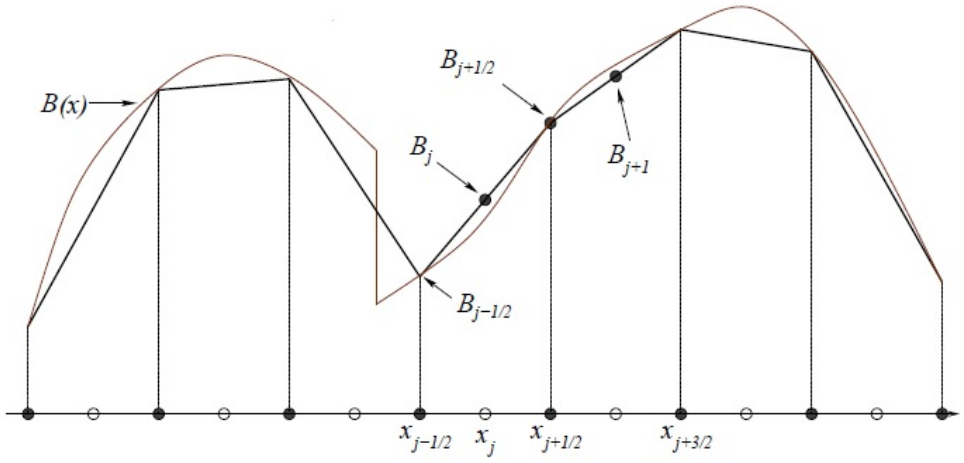

Figure 3.1: Bottom topography and its piecewise linear approximation [15]

3.2.4 Bottom or bed topography

The KP07 central-upwind scheme can also handle bed discontinuities or discontinuous bottom topography B. It achieves this by replacing the bottom topography function $B(x)$ with its piecewise linear continuous approximation $\widetilde{B}(x)$ as shown in Figure 3.1.

$$\widetilde{B}(x) = B_{j-\frac{1}{2}} + \left(B_{j+\frac{1}{2}} - B_{j-\frac{1}{2}}\right)\frac{x - x_{j-\frac{1}{2}}}{\triangle x}, \qquad x_{j-\frac{1}{2}} \le x \le x_{j+\frac{1}{2}} \tag{3.17}$$

with

$$B_{j\pm\frac{1}{2}} = \frac{B\left(x_{j\pm\frac{1}{2}} + 0\right) + B\left(x_{j\pm\frac{1}{2}} - 0\right)}{2}. \tag{3.18}$$

At $x = x_j$, $\widetilde{B}(x_j) = B_j$ gives the cell average value in the domain $x_{j-\frac{1}{2}} \le x \le x_{j+\frac{1}{2}}$. Being a piecewise linear function, it is equal to the average value at the endpoints.

$$B_j = \widetilde{B}(x_j) = \frac{1}{\triangle x}\int_{x_{j-\frac{1}{2}}}^{x_{j+\frac{1}{2}}} \widetilde{B}(x)dx = \frac{B_{j+\frac{1}{2}} + B_{j-\frac{1}{2}}}{2}. \tag{3.19}$$

In most of the cases, the cell interface/edge values of the bottom elevation $B_{j\pm\frac{1}{2}}$ is known from the geometry of the open channel. We then apply equation 3.19 to obtain the bottom elevation at the cell center.

3.2.5 Positivity preserving

The average value of the depth of the fluid at the cell center can be calculated as

$$\overline{h}_j = \overline{z}_j - B_j. \tag{3.20}$$

The use of a slope limiting function does not guarantee the positivity of the fluid depth. In cases where the reconstruction given by equation 3.8 produces negative values of h, make the slope of h equal to the slope of B (correction of the basic piecewise linear reconstruction) i.e.

$$\text{if } z^-_{j+\frac{1}{2}} < B_{j+\frac{1}{2}} \text{ or } z^+_{j-\frac{1}{2}} < B_{j-\frac{1}{2}} \text{ then } s_j = \tfrac{\partial B}{\partial x}.$$

Equivalently we obtain the following,

$$\text{if } z^-_{j+\frac{1}{2}} < B_{j+\frac{1}{2}} \text{ or } z^+_{j-\frac{1}{2}} < B_{j-\frac{1}{2}} \text{ then}$$

$$z^-_{j+\frac{1}{2}} = \overline{h}_j + B_{j+\frac{1}{2}}, \quad z^+_{j-\frac{1}{2}} = \overline{h}_j + B_{j-\frac{1}{2}}.$$

The general way of calculating the velocity is

$$u^{\pm}_{j\pm\frac{1}{2}} = \frac{q^{\pm}_{j\pm\frac{1}{2}}}{h^{\pm}_{j\pm\frac{1}{2}}} \tag{3.21}$$

with

$$h^{\pm}_{j\pm\frac{1}{2}} = z^{\pm}_{j\pm\frac{1}{2}} - B_{j\pm\frac{1}{2}}. \tag{3.22}$$

3.2.6 Desingularization

In the channel areas which are dry or almost dry (if computational domain contains dry bed, islands or coastal areas), the values of $h^{\pm}_{j\pm\frac{1}{2}}$ could be very small or even zero. If $h^{\pm}_{j\pm\frac{1}{2}}$ is very small or zero, then $u^{\pm}_{j\pm\frac{1}{2}}$ will become artificially large if it is calculated using equation 3.21. In such cases when $h^{\pm}_{j\pm\frac{1}{2}} < \epsilon$, with ϵ being an a-priori chosen small positive number (e.g. $\epsilon = 1e^{-5}$), the piecewise linear reconstruction of $U^{(2)} := q$ should be replaced with a piecewise linear reconstruction of u in the entire computational domain. At first the velocity at the cell centers in the entire domain is recomputed by the desingularization formula

$$\overline{u}_j = \frac{2\overline{h}_j \cdot \overline{q}_j}{\overline{h}_j^2 + \max\left(\overline{h}_j^2, \epsilon^2\right)}, \tag{3.23}$$

then the point values of the velocity $u^{\pm}_{j\pm\frac{1}{2}}$ at the left/right cell interfaces i.e. at $x_j = x_{j\pm\frac{1}{2}}$ are computed as

$$u^{-}_{j+\frac{1}{2}} = \overline{u}_j + \frac{\triangle x}{2} s_{u_j} \tag{3.24}$$

$$u^{+}_{j+\frac{1}{2}} = \overline{u}_{j+1} - \frac{\triangle x}{2} s_{u_{j+1}} \tag{3.25}$$

$$u^{-}_{j-\frac{1}{2}} = \overline{u}_{j-1} + \frac{\triangle x}{2} s_{u_{j-1}} \tag{3.26}$$

$$u^{+}_{j-\frac{1}{2}} = \overline{u}_j - \frac{\triangle x}{2} s_{u_j}. \tag{3.27}$$

The slope or the numerical derivative of the velocity $\left(s_{u_j}\right)$ are calculated using the same limiter function as in equation 3.15 however in this case replacing $\overline{U}$ by $\overline{u}$ (it has not been rewritten here for the sake of brevity). Finally and most importantly, the values of the discharge $q^{\pm}_{j\pm\frac{1}{2}}$ should be recomputed as

$$q^{\pm}_{j\pm\frac{1}{2}} = h^{\pm}_{j\pm\frac{1}{2}} \cdot u^{\pm}_{j\pm\frac{1}{2}}. \tag{3.28}$$

3.2.7 One-side local speeds of propagation

Once the values of $h^{\pm}_{j\pm\frac{1}{2}}$ and $u^{\pm}_{j\pm\frac{1}{2}}$ are obtained, the one-sided local speed of propagations can be estimated as the largest and the smallest eigen values of the Jacobian of the system as

$$a^{+}_{j\pm\frac{1}{2}} = \max\left\{u^{+}_{j\pm\frac{1}{2}} + \sqrt{gh^{+}_{j\pm\frac{1}{2}}}\,, u^{-}_{j\pm\frac{1}{2}} + \sqrt{gh^{-}_{j\pm\frac{1}{2}}}\,, 0\right\} \tag{3.29}$$

$$a^{-}_{j\pm\frac{1}{2}} = \min\left\{u^{+}_{j\pm\frac{1}{2}} - \sqrt{gh^{+}_{j\pm\frac{1}{2}}}\,, u^{-}_{j\pm\frac{1}{2}} - \sqrt{gh^{-}_{j\pm\frac{1}{2}}}\,, 0\right\}. \tag{3.30}$$

3.2.8 Well-balanced

The source term $\overline{S_j}(t)$ has to be appropriately discretized to ensure that the method is well-balanced. When $q := hu = 0$, then $z =$ constant and the system exhibits stationary steady state solutions (lake at rest condition). Obviously for $q := hu \neq 0$, the system has a particular nontrivial steady state solution such that $hu =$ constant, $h =$ constant. A well balanced scheme should use the quadrature formula for $\int_{x_{j-\frac{1}{2}}}^{x_{j+\frac{1}{2}}} S\,dx$ such that it is of second order and

$$\overline{S}_j(t) \approx \frac{1}{\triangle x}\int_{x_{j-\frac{1}{2}}}^{x_{j+\frac{1}{2}}} S dx = \frac{H_{j+\frac{1}{2}}(t) - H_{j-\frac{1}{2}}(t)}{\triangle x} \tag{3.31}$$

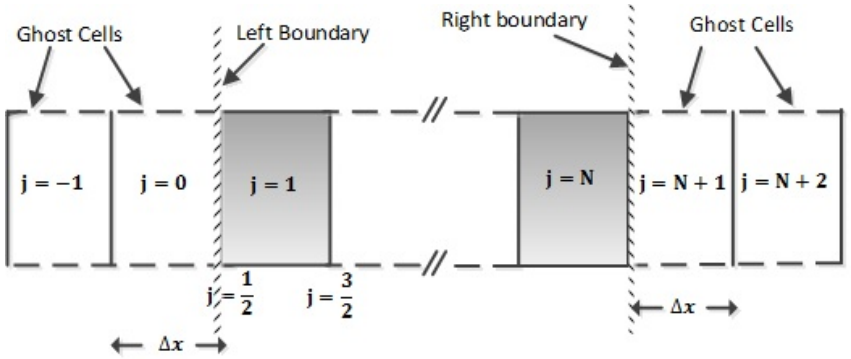

Figure 3.2: Ghost cells at the grid boundaries

i.e. the flux integrals should be cancelled out by the source term at the stationary steady state. The detailed formulation and the development of such a quadrature rule can be found at [14]. The first part of $\overline{S}_j^{(2)}(t)$ (the bed slope part) can be written as

$$\overline{S}_j^{(2),1}(t) \approx -g\left(\overline{z}_j - B_j\right)\frac{B_{j+\frac{1}{2}} - B_{j-\frac{1}{2}}}{\triangle x}. \tag{3.32}$$

The second part of $\overline{S}_j^{(2)}(t)$ (the friction part) can be computed using the same desingularization procedure as in equation 3.23 as

$$\overline{S}_j^{(2),2}(t) \approx -\frac{gn^2\overline{q}_j\left|\overline{q}_j\right|\left(w + 2(\overline{z}_j - B_j)\right)^{\frac{4}{3}}}{w^{\frac{4}{3}}} \cdot \left(\frac{2(\overline{z}_j - B_j)}{(\overline{z}_j - B_j)^2 + \max\left((\overline{z}_j - B_j)^2, \epsilon^2\right)}\right)^{\frac{7}{3}}. \tag{3.33}$$

3.3 Ghost cells

From equations 3.11 - 3.15, it can be observed that for a given j^{th} cell, information from the neighbouring cells $j-1$ and $j-2$ (to the left) and $j+1$ and $j+2$ (to the right) are required for calculating the flux integrals. This will pose difficulties at the cells on the left and right boundaries of the open channel. While evaluating the flux integrals near the left boundary cells ($j = 1$ and $j = 2$) and near the right boundary cells ($j = N-1$ and $j = N$, N being the number of cells in the grid), imaginary cells that lie outside the physical boundary of the open channel should be taken into consideration as shown in Figure 3.2.

These imaginary cells denoted by $j = 0$ and $j = -1$ on the left, and $j = N+1$ and $j = N+2$ on the right are called ghost cells. The average value of the conserved variables at the center of these ghost cells depend on the nature of the physical boundary of the channel taken into account. Various boundary conditions such as the Neumann

boundary conditions and the Dirichlet boundary conditions can be applied to obtain the ghost cells values.

For a transmissive left boundary, one simple possibility for $\overline{z}_{j=0}$ would be

$$\begin{aligned} \overline{h}_{j=0} &= 2\overline{h}_{j=1} - \overline{h}_{j=2} && (3.34)\\ \overline{z}_{j=0} &= \overline{h}_{j=0} + B_{j=0}, && (3.35) \end{aligned}$$

and for $\overline{z}_{j=-1}$

$$\begin{aligned} \overline{h}_{j=-1} &= 2\overline{h}_{j=0} - \overline{h}_{j=1} && (3.36)\\ \overline{z}_{j=-1} &= \overline{h}_{j=-1} + B_{j=-1}. && (3.37) \end{aligned}$$

For the values of $q_{j=0}$ and $q_{j=-1}$, one possibility would be

$$\begin{aligned} \overline{q}_{j=0} &= 2\overline{q}_{j=1} - \overline{q}_{j=2} && (3.38)\\ \overline{q}_{j=-1} &= 3\overline{q}_{j=1} - 2\overline{q}_{j=2}. && (3.39) \end{aligned}$$

Similarly for a transmissive right boundary, for $\overline{z}_{j=N+1}$ we have

$$\begin{aligned} \overline{h}_{j=N+1} &= 2\overline{h}_{j=N} - \overline{h}_{j=N-1} && (3.40)\\ \overline{z}_{j=N+1} &= \overline{h}_{j=N+1} + B_{j=N+1}, && (3.41) \end{aligned}$$

and for $\overline{z}_{j=N+2}$

$$\begin{aligned} \overline{h}_{j=N+2} &= 2\overline{h}_{j=N+1} - \overline{h}_{j=N} && (3.42)\\ \overline{z}_{j=N+2} &= \overline{h}_{j=N+2} + B_{j=N+2}. && (3.43) \end{aligned}$$

For the values of $q_{j=N+1}$ and $q_{j=N+2}$, one possibility would be

$$\begin{aligned} \overline{q}_{j=N+1} &= 2\overline{q}_{j=N} - \overline{q}_{j=N-1} && (3.44)\\ \overline{q}_{j=N+2} &= 3\overline{q}_{j=N} - 2\overline{q}_{j=N-1}. && (3.45) \end{aligned}$$

The values of $B_{j=0}$, $B_{j=-1}, B_{j=N+1}$ and $B_{j=N+2}$ can be obtained by extending the geometry of the channel at each ends.

Chapter 4

Application

4.1 Introduction

The KP07 central-upwind scheme can be used for various applications as a black box solver. However, in this chapter, to provide an example of the application of the scheme, a river flow simulation is presented.

4.2 Example of a river flow

Trinnelva is a river in eastern Norway that flows through a town called Notodden. It flows out of lake Tinnsjøen. There are several hydropower stations along the length of the river. We will focus our attention to the part of the river the lies between Årlifoss and Grønvollfoss hydropower stations. A birds eye view of the river and the surrounding area is shown in Figure 4.1. The topography of the river bed and the elevation of the free water surface is schematically shown in Figure 4.2.

The river is 5 km in length. The difference in the elevation of the river bed between the left and right boundaries is 17.5 m. There is a steeper drop of the river bed at 2.5 km distance from Årlifoss power station (left boundary).

4.2.1 Simulation scenario

The volumetric flowrate of the water entering the part of the river (at the left boundary) can be controlled[1] at the Årlifoss power station. Similarly, the volumetric flowrate of the water leaving the part of the river (at the right boundary) can be controlled at the Grønvollfoss power station. The nominal flowrate of water at these power stations is 120 m^3/s. The nominal depth of the water at Grønvollfoss is about 17.08 m and at Årlifoss is about 0.5 m. If the flowrate of the water (inflow) at Årlifoss is changed from 120 m^3/s to 160 m^3/s for 15 minutes, it is of interest to observe the following:

[1] The flowrate of the water can be changed by altering the power production. In general, in a hydro power station, guide vanes are closed/opened to control the flowrate.

Figure 4.1: Trinnelva in Notodden

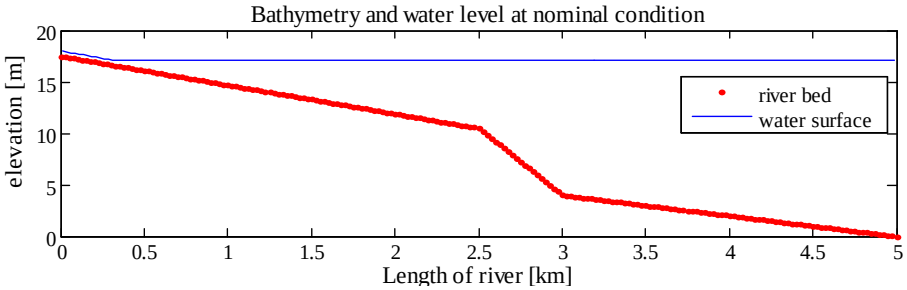

Figure 4.2: Bottom topography and surface elevation

Table 4.1: Parameters of the river flow system

Parameters	**Value**	**Description**	**Unit**
L	5	Length of river	km
V_{in}	120	Inflow	m^3/s
V_{out}	120	Outflow	m^3/s
w	180	Constant channel width	m
$\triangle x$	25	cell size	m
θ	1.3	dissipation tuner	$-$
ϵ	1e-8	small positive number	$-$
n	0.04	Manning's roughness coefficient	$s/m^{\frac{1}{3}}$

a) How long does it take the wave to travel from Årlifoss to Grønvollfoss?

b) If the outflow at Grønvollfoss is kept constant at 120 m^3/s, how does the level of the water at Grønvollfoss change?

Table 4.1 lists the values of the parameters of the river system. MATLAB is used as the simulation tool. For solving the ODE's, the built-in MATLAB ode solvers are used (with an assumption that they are TVD preserving).

4.2.2 Simulation results

The central-upwind scheme of Kurganov and Petrova is used to simulate the river flow. At the simulation time of $t = 10$ min, the inflow at Årlifoss is increased from 120 m^3/s to 160 m^3/s. At $t = 25$ min, the inflow is decreased back to 120 m^3/s. This can also be depicted in the lower part of Figure 4.3. The level of the river and the average volumetric flow rate in the first cell of the grid are shown in Figure 4.3. A wave is formed at the first cell (at Årlifoss) of the grid (see upper figure of Figure 4.3) and this wave travels downstream towards Grønvollfoss.

However, from Figure 4.4 it can be clearly seen that the level of the water at Grønvollfoss starts to increase only at about $t = 20.5$ min. This means that it takes about 10.5 min for the first wave to hit the right boundary of the grid at Grønvollfoss.The first wave will be reflect back at Grønvolfoss because of which the level once again start to decrease (at about $t = 38$ min). A second wave (with a smaller amplitude than the first wave) arrives at the right boundary and reaches its peak (at about $t = 50$ min). It gets reflected back again. This process repeats until the system attains a new steady state level of about 17.2 m at Grønvollfoss as shown in Figure 4.4. Due to the inflow of water into the channel from Årlifoss for 15 minutes, the level of the water at Grønvollfoss increases by about 4 cm.

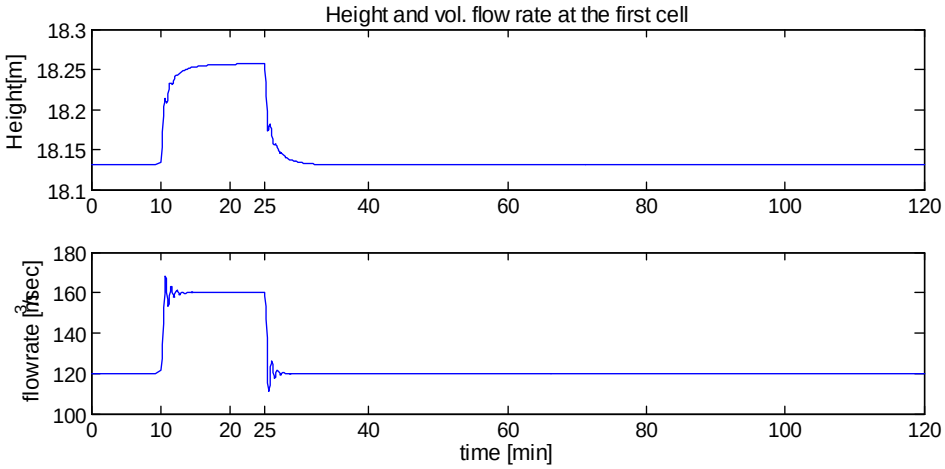

Figure 4.3: Height and volumetric flow rate at the first cell of the grid

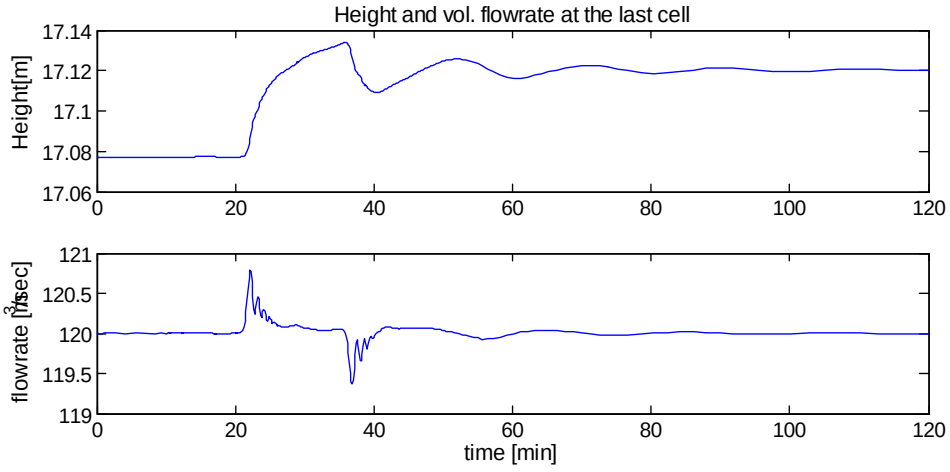

Figure 4.4: Height and volumetric flow rate at the last cell (Grønvollfoss)

Bibliography

[1] X.-D. Liu, E. Tadmor, Third order nonoscillatory central scheme for hyperbolic conservation laws, Numerische Mathematik 79 (1998) 397–425.

[2] A. Kurganov, G. Petrova, A third-order semi-discrete genuinely multidimensional central scheme for hyperbolic conservation laws and related problems, Numerische Mathematik 88(4) (2001) 683–729.

[3] A. Harten, B. Engquist, S. Osher, S. R. Chakravarthy, Uniformly high order accurate essentially non-oscillatory schemes, iii, Journal of Computational Physics 131 (1997) 3–47.

[4] C.-W. Shu, Numerical experiments on the accuracy of eno and modified eno schemes, Journal of Scientific Computing 5(2) (1990) 127–149.

[5] X.-D. Liu, S. Osher, T. Chan, Weighted essentially non-oscillatory schemes, Journal of Computational Physics 115(1) (1994) 200–212.

[6] G.-S. Jiang, C.-W. Shu, Efficient implementation of weighted eno schemes, Journal of Computational Physics 126 (1996) 202–228.

[7] D. Levy, G. Puppo, G. Russo, Central weno schemes for hyperbolic systems of conservation laws, ESAIM: Mathematical Modelling and Numerical Analysis 33(03) (1999) 547–571.

[8] D. Levy, G. Puppo, G. Russo, Compact central weno schemes for multidimensional conservation laws, SIAM Journal on Scientific Computing 22(2) (2000) 656–671.

[9] S. K. Godunov, Different mmethod for shock waves, Ph.D. thesis, Moscow State University (1954).

[10] K.-A. Lie, S. Noelle, On the artificial compression method for second order nonoscillatory central difference schemes for system of conservation laws, SIAM 24 (2003) 1157–1174.

[11] H. Nessyahu, E. Tadmor, Non-oscillatory central differencing for hyperbolic conservation laws, Journal of Computational Physics 87(2) (1990) 408–463.

[12] P. K. Sweby, High resolution schemes using flux limiters for hyperbolic conservation laws, SIAM Journal on Numerical Analysis 21(5) (1984) 995–1011.

[13] A. Kurganov, S. Noelle, G. Petrova, Semidiscrete central-upwind schemes for hyperbolic conservation laws and hamilton-jacobi equations, SIAM Journal on Scientific Computing 23(3) (2000) 707–740.

[14] A. Kurganov, D. Levy, Central-upwind schemes for the saint venant system, ESAIM: Mathematical Modelling and Numerical Analysis 36(2) (2002) 397–425.

[15] A. Kurganov, G. Petrova, A second order well-balanced positivity preserving central-upwind scheme for the saint-venant system, Communications in Mathematical Sciences 5(1) (2007) 133–160.

[16] A. Chertock, S. Chi, A. Kurganov, T. Wu, Well-balanced positivity preserving central-upwind scheme for the shallow water system with friction terms, International Journal for numerical methods in fluids 78 (2015) 355–383.